# COMPRESSION AND TORSION BUCKLING TESTS ON FIBER COMPOSITE CYLINDERS

**Chiara Bisagni**

Dipartimento di Ingegneria Aerospaziale
Politecnico di Milano
Via La Masa 34, 20158 Milano, Italy
e-mail: Chiara.Bisagni@polimi.it

## 1. Abstract

The work presented in this paper is part of a larger research project aiming at improving the knowledge of the buckling behaviour of composite shell structures. In particular, the paper deals with experimental buckling tests of carbon fiber reinforced plastics (CFRP) thin-walled cylindrical shells under axial compression and torsion.
Indeed a solution seems not well indicated till now for the buckling strength prediction of composite shell structures. Consequently, the efficient use of composite shells has been generally restricted by the limited availability of buckling design criteria.
In this work, CFRP cylindrical shells with different types of lay-up orientation are experimentally tested under axial compression and torsion, using a position control mode. During the tests, an equipment with five laser displacement sensors allows to measure both the initial geometric imperfections and the buckling pattern development on the specimens internal surfaces.

## 2. Introduction

The rotorcrafts have been among the first flying machines adopting structural components made by composite materials [1]. Some very important problems, such as fatigue in rotor blades, have been well identified and almost completely solved, while for others a solution seems not well indicated till now. This is particularly true in the case of buckling strength prediction of composite shell structures, as thin-walled circular cylindrical shells, that constitute primary structural parts, such as helicopter tailboom.
Indeed, the studies regarding the buckling phenomena of composite cylindrical shells result much more complicated than in the case of isotropic shells and they have not yet led to systematic and widely applicable design criteria [2-7].
In the past few decades, the dominant role of initial imperfections in causing specific shell configurations, particularly circular cylindrical configurations subject to axial compression, to buckle at a load level considerably lower than the value predicted by the classical linearised small deflection theory has been recognised and accepted also for composite shells. As a matter of fact, the buckling of composite shells depends also on a large number of input parameters, such as laminae properties and orientations. The phenomenon can be also influenced by several types of imperfections, consequences of the manufacturing process, such as thickness variations and local delaminations.
A methodology, integrating a reasonable number of experimental tests with a complementary computational activity, appears as the only possible approach to investigate this phenomenon. Indeed, the very large number of input parameters prohibits a pure experimental approach, but, in the meantime, the measurement of relevant properties and response parameters during testing is essential to the development of analytical/numerical procedures and design guidelines for the buckling strength prediction [8-10].
The work presented in this paper is part of a larger research project aiming at improving the knowledge of the buckling behaviour of composite shell structures [10-12]. In particular, the paper deals with experimental buckling tests of CFRP thin-walled cylindrical shells under axial compression and torsion, using a position control mode.
This study can contribute to a better definition of applicable strength design criteria for composite shells in buckling and post-buckling, with the final aim of a larger structure weight saving.

## 3. Cylindrical shells

The specimens considered in this study were produced by Agusta from carbon fiber reinforced plastics (CFRP) laminates, using traditional hand lay-up on a mandrel.
The specimens (Figure 1) are characterised by an internal diameter and an overall length of 700 *mm*, comprising two tabs provided at the top and at the bottom surfaces, for attaching them to the loading rig. The actual length is therefore limited to the central part and is equal to 520 *mm*. The nominal thickness of all the specimens is 1.32 *mm* with a nominal radius-to-thickness ratio of 265.
The specimens considered in this study present two different stacking sequences: [0°/45°/-45°/0°] and [45°/-45°]s. Mechanical property tests for CFRP ply were carried out by Agusta and the results are presented in Table 1.

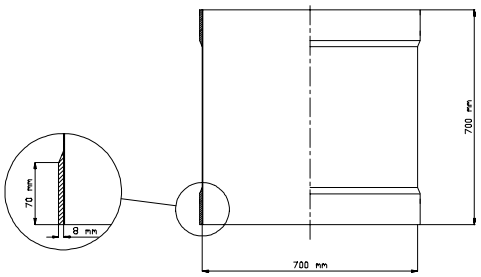


Figure 1 - Cylindrical specimen

| | |
|---|---|
| $E_{11}$ $E_{22}$ *[N/mm²]* | 52000 |
| $G_{12}$ $G_{13}$ $G_{23}$ *[N/mm²]* | 2350 |
| $\nu_{12}$ | 0.302 |

Table 1 - Properties of the specimens layers

## 4. Buckling tests equipment

The experimental buckling tests are performed on the CFRP cylindrical shells under axial compression and torsion, by a loading rig using a position control mode (Figure 2).
To perform axial compression tests, the loading platform is pushed by a hydraulic ram against four ball screw supports placed at the four corners of the platform. At the beginning, the load given by the ram is completely supported by the four screws, which distribute the real applied load on the specimen during the test. In fact, the screws motion is computer-controlled, producing exactly the desired displacement to the loading platform, by means of four stepping motors through four reduction gears. Thus the load level, which is transferred smoothly to the cylinder, depends only on the platform displacement and on the cylinder elastic response and it does not substantially depend on the load magnitude due to the hydraulic ram acting on the platform.
The compression load is measured, during the tests, by means of a load cell situated under the lower clamp, while three LVDT transducers measure the axial displacement of the specimen at three equally spaced points.
To perform torsion tests, the rotation is given to the specimen bottom by means of a torsion lever. The lever motion is computer-controlled, producing the desired displacement of a screw by means of a stepping motor through a reduction gear, like in the case of axial compression. The load cell, situated under the lower clamp, is able to measure also the torsion, while three LVDT transducers measure the tangential displacement of the specimen bottom at the same three points used during axial compression.

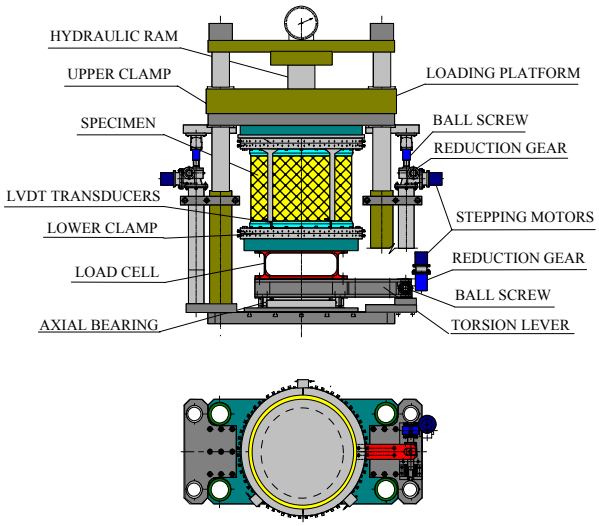


Figure 2 - Equipment for the buckling tests

## 5. Equipment for the measurements of the geometric imperfections and post-buckling pattern

An equipment (Figure 3) was designed to measure the geometric imperfections and the development of the post-buckling pattern on the specimens internal surface during the tests.
The equipment is placed inside the specimen during the tests and employs five laser displacement sensors to measure the specimens internal surface, so to avoid any contact with the specimen and consequently not to influence the buckling behaviour.
The five laser displacement sensors are fixed on a slide, capable of rotating and vertically translating. The combination of the two movements allows to

measure the all internal surface of the specimens. These movements are generated by two stepping motors and the vertical position of the slide is determined by an incremental encoder. The laser displacement sensors are placed at the distance of 40 *mm* from the specimen internal surface. They guarantee a measurement range of ±10 *mm* with a resolution of 15 $\mu m$, for recording of both the geometric imperfections (some tens of micrometers) and the buckling pattern (about 10 - 20 *mm*). The measurements are recorded in a regular mesh of points 10 *mm* spaced both circumferentially and axially.

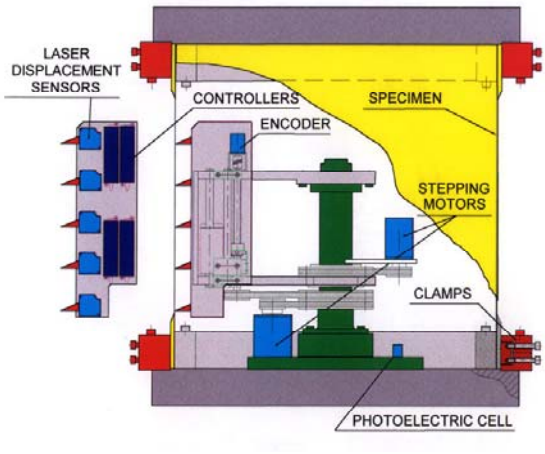


Figure 3 – Equipment for the measurement of the geometric imperfections and the post-buckling pattern

Detailed measurement of the initial geometric imperfections are carried out, using the laser scanning system, after each specimen is mounted in the test rig and before any load is applied. The data are processed according to a best-fit procedure, originally developed by Arbocz and Babcock [9] and then used by other authors [12-13], because it facilitates comparative studies on the effect of the manufacturing process on the magnitude and spatial distribution of initial imperfections.
The initial geometric imperfections measured on a test specimen at three different height of the cylinder (one quarter, half and three quarter of the height) are presented in Figure 4 in a polar diagram with an amplification factor equal to 70. The measured initial geometric imperfections present a mean value of imperfection amplitude equal to 0.084 *mm*, that corresponds to a ratio between imperfection amplitude and shell thickness equal to 0.063.

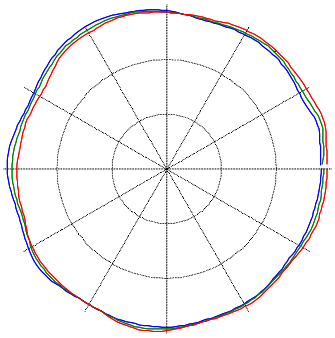

Figure 4 – Typical polar diagram of measured initial imperfections

These data of the geometric imperfections, measured by laser sensors on the specimens internal surface are useful to be introduced into the finite element models to evaluate the influence of the geometric imperfections on the buckling loads.
The equipment allows then to measure the pre-buckling and post-buckling patterns on the cylinders internal surface during the tests itself. Normally the surface is measured 15-20 times during each test. Indeed the time required to measure a complete surface is limited to 4 minutes.
The all experimental equipment is computer-controlled by means of a software ad-hoc developed in *Visual Basic,* through two multifunction acquisition boards. The first one controls the buckling tests equipment, giving the stepping motors commands and acquiring the measurements of the load cell and the LVDT transducers. The second board controls the equipment for the measurements of the cylinders internal surface.

## 6. Results of the buckling tests under axial compression

The specimens are axially compressed, recording the compression load vs. the axial displacement and the development of the post-buckling pattern.
The values of the measured buckling loads are reported in Tables 2 and 3, where they are compared to the analytical buckling loads, obtained from a classical linear theory, not including the effect of the initial imperfections [14].
The ratio between the experimental buckling load and the analytical one is higher for the $[45°/-45°]_S$ cylinders than for the [0°/45°/-45°/0°] cylinders.
Tables 2 and 3 also report the post-buckling pattern number of waves, in the circumferential and axial direction respectively. Cylinders with the same lay-up orientation develop a post-buckling pattern that is quite always the same. On the other side, cylinders

with different lay-up orientation show significant differences on the post-buckling pattern.

| Cylinder number | Exp. load *[kN]* | Analyt. load *[kN]* | Exp. / analyt. load | Post-buckl. pattern |
|---|---|---|---|---|
| 1st | 172.87 | 240 | 0.72 | 9 x 2 |
| 2nd | 151.62 | | 0.63 | 10 x 2 |
| 3rd | 155.67 | | 0.65 | 10 x 2 |
| 4th | 164.70 | | 0.69 | 10 x 2 |

Table 2 - Axial compression buckling loads: [0°/45°/-45°/0°] cylinders

| Cylinder number | Exp. load *[kN]* | Analyt. load *[kN]* | Exp. / analyt. load | Post-buckl. pattern |
|---|---|---|---|---|
| 1st | 120.23 | 120.58 | 0.99 | 8 x 1 |
| 2nd | 116.45 | | 0.97 | 7 x 1 |
| 3rd | 102.45 | | 0.85 | 8 x 1 |
| 4th | 112.63 | | 0.93 | 8 x 1 |

Table 3 - Axial compression buckling loads: $[45°/-45°]_S$ cylinders

Two typical diagrams of compression load vs. axial displacement are presented in Figures 5 and 6, where both loading and unloading sequences are reported. In the tests on the [0°/45°/-45°/0°] cylinders, the buckling load is reached without significant pre-buckling nonlinearities, while pre-buckling non-linearities are present during the tests on the $[45°/-45°]_S$ cylinders.

All the tests performed show that the buckling phenomena under axial compression appear suddenly and in any case a load reduction is measured. The tests are continued for a little in the post-buckling field, leading to further increase of load and displacement. During the unloading phase, the diagrams agree with the theoretical curves, until the buckling patterns disappear and the values return to coincide with those of the loading sequence.

Figures 7 and 8 report the post-buckling patterns recorded during two tests under axial compression. The patterns are well defined and perfectly regular. They do not change during the tests, but there is only an increase of the displacements normal to the surface, in the post-buckling region.

For the [0°/45°/-45°/0°] cylinder, it is possible to point out 9 circumferential waves and 2 axial waves and the displacements normal to the surface reach 11 *mm* internally and 5 *mm* externally in the post-buckling region. The pattern recorded during a test on a $[45°/-45°]_S$ cylinder shows 8 circumferential waves and 1 axial wave. The displacements normal to the surface reach, in the post-buckling region, 14 *mm* internally and 7 *mm* externally.

A photograph of a typical post-buckling pattern for a CFRP cylinder, as it appears during a test in the post-buckling field, is reported in Figure 9.

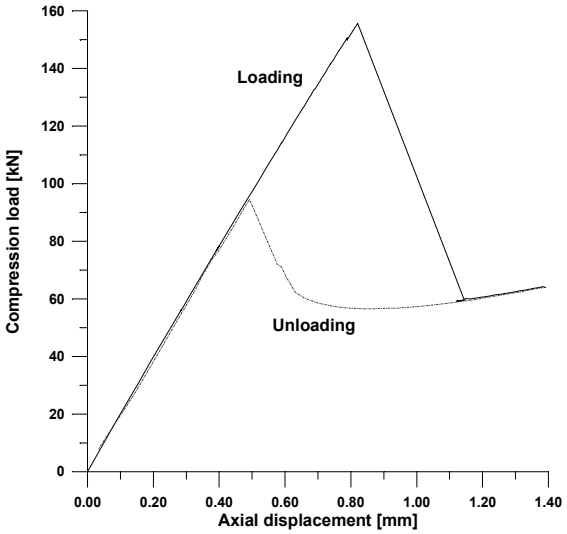


Figure 5 - Compression load vs. axial displacement: [0°/45°/-45°/0] cylinder

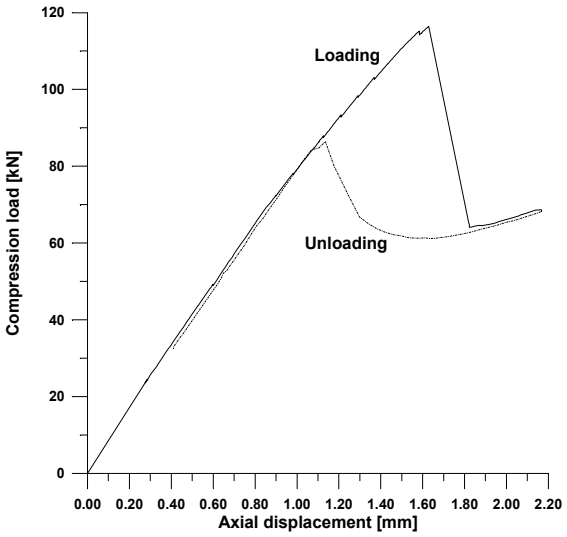


Figure 6 - Compression load vs. axial displacement: [45°/-45°]s cylinder

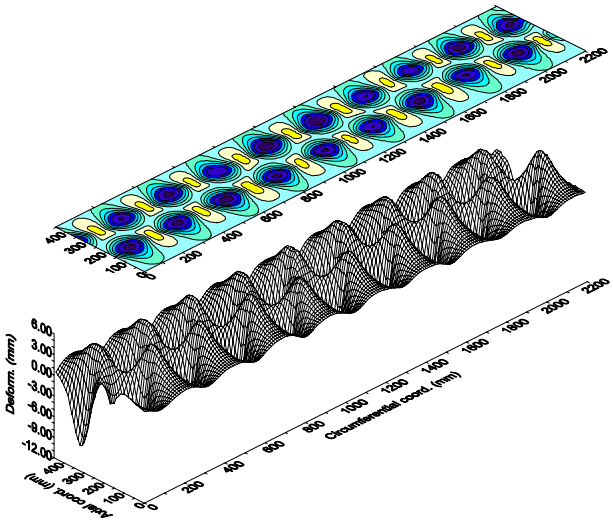


Figure 7 - Typical post-buckling pattern for a [0°/45°/-45°/0°] cylinder under axial compression

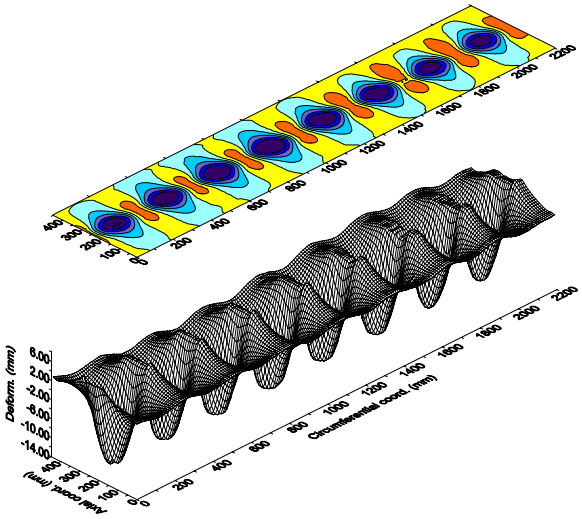


Figure 8 - Typical post-buckling pattern for a [45°/-45°]s cylinder under axial compression

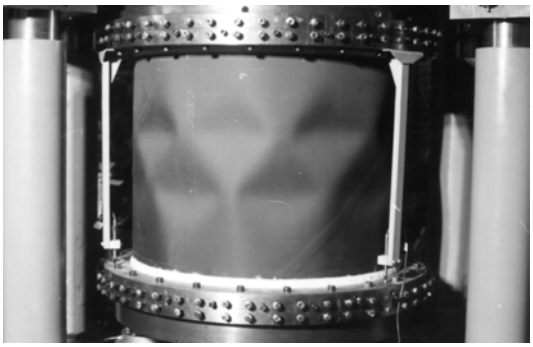

Figure 9 – Photo of a typical post-buckling pattern under axial compression

## 7. Results of the buckling tests under torsion

The specimens are then tested under torsion. During the tests the torsion torque vs. the rotation angle are recorded as well as the evolution of the post-buckling pattern.
The values of the measured buckling torques are reported in Table 4, where also the post-buckling pattern number of waves is reported.

| Cylinder lay-up | Exp. torque *[Nm]* | Post-buckl. pattern |
|---|---|---|
| [0°/45°/-45°/0°] | 14300 | 12 |
| $[45°/-45°]_S$ | 9100 | 11 |

Table 4 – Torsion buckling torques

Two typical diagrams of torsion torque vs. rotation angle are presented in Figures 10 and 11, where both loading and unloading sequences are reported.
All the tests performed show that buckling phenomena appear slowly and no great stiffness reduction is measured. The tests are continued for a little in post-buckling field, leading to further increase of torque and rotation. During the unloading phase, when the buckling patterns disappear, the values return to coincide with those of the loading sequence.
Figures 12 and 13 report the post-buckling patterns recorded during two tests under torsion. The patterns are well defined and do not change during the tests, but there is only an increase of the displacements normal to the surface, in the post-buckling region.
For the [0°/45°/-45°/0°] cylinder, it is possible to point out 12 waves and the displacements normal to the surface reach 11 *mm* internally and 3 *mm* externally in the post-buckling field. The pattern recorded during a test on a $[45°/-45°]_S$ cylinder shows 11 waves and the displacements normal to the surface reach, in the post-buckling region, 14 *mm* internally and 5 *mm* externally.
A photograph of a typical post-buckling pattern for a CFRP cylinder under torsion, as it appears during a test in the post-buckling field, is reported in Figure 14.

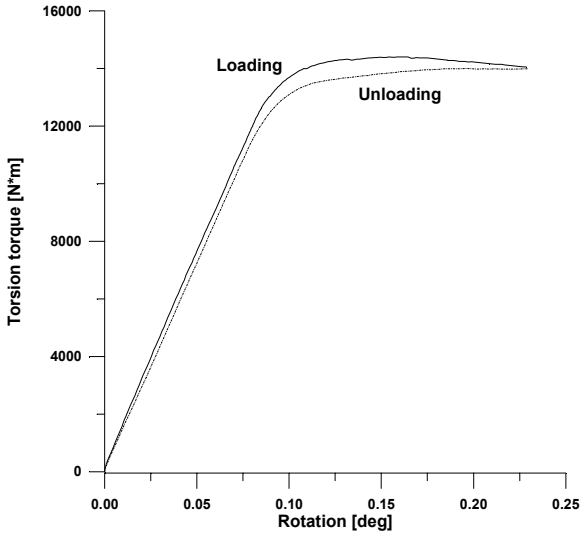


Figure 10 – Torsion torque vs. rotation: [0°/45°/-45°/0] cylinder

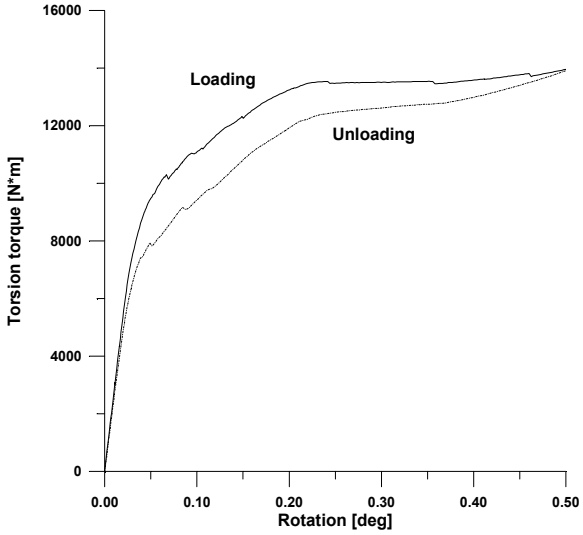


Figure 11 – Torsion torque vs. rotation: [45°/-45°]s cylinder

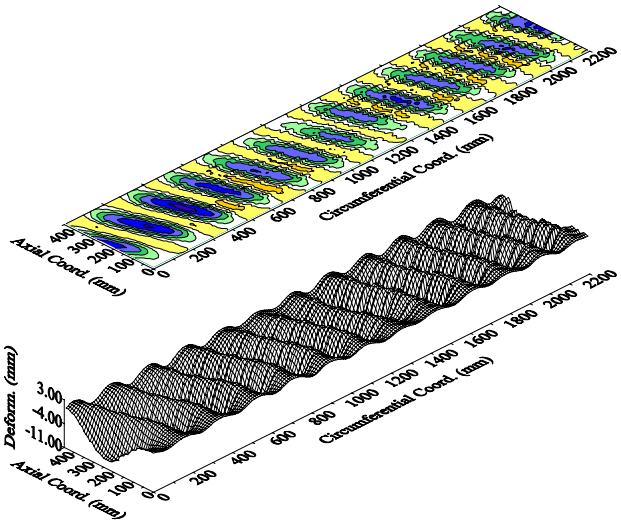


Figure 12 - Typical post-buckling pattern for a [0°/45°/-45°/0°] cylinder under torsion

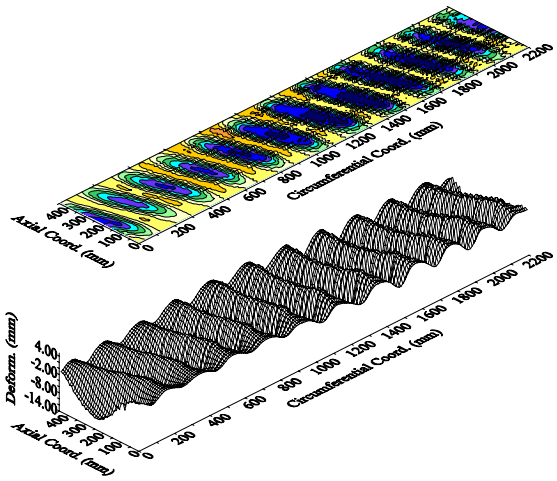


Figure 13 - Typical post-buckling pattern for a [45°/-45°]s cylinder under torsion

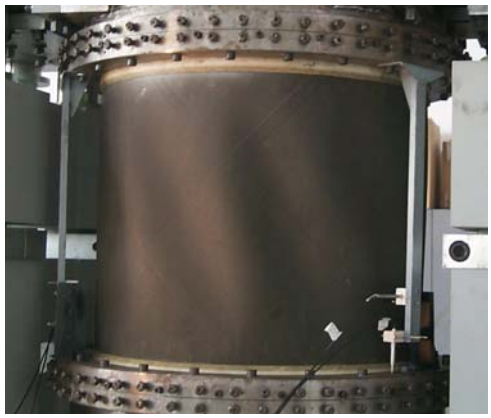

Figure 14 – Photo of a typical post-buckling pattern under torsion

## 8. Conclusions

The results of an experimental investigation of the buckling and post-buckling behaviour of CFRP thin-walled cylindrical shells have been presented.
Experimental buckling tests have been performed under axial compression and torsion, using a position control mode.
During the tests, the compression load vs. the axial displacement and the torsion torque vs. the rotation angle are measured by means of a load cell and LVDT transducers. Besides an ad-hoc equipment allows to measure, on the specimens internal surfaces, the initial geometric imperfections and the evolution of the post-buckling pattern. The measurements are taken by means of five laser displacement sensors.
The experimental results are fundamental to set-up finite element models, having the same characteristics as the real specimens and being able to reproduce the results of the experimental tests, i.e. both the buckling load values and the post-buckling behaviours. These validated models are useful to understand the conditions that mainly influence the buckling phenomena under axial compression and torsion and to perform a wide sensitivity study, fundamental to the definition of strength design criteria.
Work is then currently under way on performing buckling tests under axial compression and torsion applied in combination.

## 9. References


1. Hiddleton D. H., *The first fifty years of composite materials in aircraft construction*, Aeronautical Journal, vol. 96, 1992.
2. Koiter W. T., *On the stability of elastic equilibrium*, Delft: Doctoral Thesis, 1945. English translation: AFFDL-TR-70 25, 1970.
3. Elishakoff I. and Arbocz J., "Reliability of axially compressed cylindrical shells with general nonsymmetric imperfections", *Journal of Applied Mechanics*, vol. 52, pp. 122-128, 1985.
4. Simitses G. J., "Buckling and postbuckling of imperfect cylindrical shells: A Review", *Applied Mechanics Reviews*, vol. 39, no. 10, pp. 1517-1524, 1986.
5. Abramovich H., Yaffe R. and Singer J., "Evaluation of stiffened shell characteristics from imperfection measurements", *Journal of Strain Analysis*, vol. 22, no. 1, pp. 17-23, 1987.
6. Simitses G.J., Shaw D. and Sheinman I., "Stability of imperfect laminated cylinders: a comparison between theory and experiments", *AIAA Journal*, vol. 23, no. 7, pp. 1086-1092, 1985.
7. Juillien J. F. et al., *Buckling of shell structures on land, in the sea and in the air*, Lyon Symposium, Elsevier Applied Science, 1991.
8. Arbocz J. and Hol J. M. A. M., "The role of experiments in improving the computational models for composite shells", Proc. of *Winter Annual Meeting of American Society of Mechanical Engineers on Analytical and Computational Models of Shells*, San Francisco, 1989.
9. Arbocz J. and Babcock C.D., "Prediction of buckling loads based on experimentally measured initial imperfections", in *Buckling of structures*, edit by Budiansky B., Berlin: Springer 1976.
10. Bisagni C., "Numerical analysis and experimental correlation of composite shell buckling and post-buckling", *Composites Part B: Engineering*, vol. 31, no. 8, pp. 655-667, 2000.
11. Bisagni C., "Carbon-epoxy laminated cylindrical shells under axial compression", Proc. of *23rd European Rotorcraft Forum*, Dresden (Germany), 1997.
12. Bisagni C., "Experimental buckling of thin composite cylinders in compression", *AIAA Journal,* vol. 37, no. 2, pp. 276-278, 1999.
13. Chryssanthopoulos M.K., Giavotto V. and Poggi C., "Characterization of manufacturing effects for buckling-sensitive composite cylinders", *Composites Manufacturing*, vol. 6, no. 2, pp. 93-101, 1995.
14. Bisagni C., *Instabilità e comportamento post-critico di gusci in materiale composito*, Ph.D. thesis (in Italian), Dipartimento di Ingegneria Aerospaziale, Politecnico di Milano, 1997.